ACKNOWLEDGMENTS

Our thanks go to Professor A. Blanc-Lapierre for extending to us the facilities of the Orsay Laboratory. We wish to thank G. Brochard and F. Richard for assistance in data taking, G. Bouvard and G. Lissilour for help in the installation of the experiment. Two of us (C.B. and J.P-Y-J) are grateful to Dr. Nguyen Ngoc for assistance in the design and test of the Čerenkov counter. We are grateful for the help provided by the technological group directed by V. Round and by the accelerator team directed by Dr. Burnod and Dr. Milman.

PHYSICAL REVIEW VOLUME 172, NUMBER 5 25 AUGUST 1968

Strange-Particle Production in 8-BeV/c Proton-Proton Interactions*†

M. FIREBAUGH,‡ G. ASCOLI, E. L. GOLDWASSER, R. D. SARD, AND J. WRAY
Department of Physics, University of Illinois, Urbana, Illinois
(Received 18 December 1967)

A systematic survey of strange-particle final states produced by 8-BeV/c protons was made in the BNL 80-in. hydrogen bubble chamber. Cross sections were measured for some 33 reactions. The ratio of the cross section for the $K\bar{K}$ channels to the total strange-particle cross section was measured to be 0.12 and appears to be rising in this momentum region. The total cross section for strange-particle production is estimated as 1.8±0.2 mb. Comparison is made of the data with the predictions of the one-pion-exchange model, and at least partial agreement occurs for the $K^+p\Lambda$ and $\pi KN\Sigma$ final states. The $Kp\Sigma$ states appear to contain $N^*(1924)\to K\Sigma$, and the $\pi KN\Lambda$ states all include $Y^*(1385)$ production with the $\pi^+K^0p\Lambda$ state also containing $N^*(1236)$ and $K^*(890)$ production. An examination of the five- and six-body K,Λ states indicates strong $Y^*(1385)$ and $N^*(1236)$ production. Finally, all final states containing a K and a Λ show a dependence on $M(K,\Lambda)$ which is well parametrized by a Breit-Wigner shape with $M_0=1777$ MeV and $\Gamma=345$ MeV. This behavior is interpreted as being consistent with one-pion exchange as the dominant mechanism for these reactions.

I. INTRODUCTION

PREVIOUS experiments on strange particles produced in p-p interactions have been reported at lower momenta (up to 6.6 BeV/c)[1] and certain topologies of strange-particle events have been examined at higher momenta (10 and 24.5 BeV/c).[2] The present experiment was initiated for several reasons: to test the extent to which one-pion exchange (OPE) contributes in this unexplored momentum region, to examine the 2-baryon mass spectra for possible $B=2, S=-1$ resonances,[3] and to determine the amount of production of the well-known resonances. The data for the experiment consisted of about 37 000 pictures of the Brookhaven 80-in. hydrogen bubble chamber exposed to 7.87 BeV/c protons at the AGS.[4]

II. ANALYSIS PROCEDURE

A. Scanning and Measuring

The entire film was scanned once in all three views and a second time in either two or three views. The events of interest were 2-, 4-, or 6-prong interactions with one or more associated kinks or V's. When such

* Work supported in part by the U. S. Atomic Energy Commission.

† Portions of this work were presented by M. Firebaugh as a thesis to the Department of Physics of the University of Illinois in partial fulfillment of the requirements for the Ph.D. degree.

‡ Present address: Department of Physics, University of Wisconsin, Madison, Wisc.

[1] Previous $p+p\to$ (strange particle) experiments at momenta <8 BeV/c: 3.68 BeV/c, R. I. Louttit, T. W. Morris, D. C. Rahm, R. R. Rau, A. M. Thorndike, and W. J. Willis, Phys. Rev. **123**, 1465 (1961); 5.0 BeV/c, E. Bierman, A. P. Colleraine, and U. Nauenberg, *ibid.* **147**, 922 (1966); 5.5 BeV/c, G. Alexander, O. Benary, N. Kidron, A. Shapira, R. Yaari, and G. Yekutieli, Phys. Rev. Letters **13**, 355A (1964); 5.4 and 6.6 BeV/c, William Dunwoodie, William E. Slater, Harold K. Ticho, Gerald A. Smith, Arthur B. Wicklund, and Stanley G. Wojcicki (unpublished); 6.0 BeV/c, W. Chinowsky, R. R. Kinsey, S. L. Klein, M. Mandelkern, J. Schultz, F. Martin, M. L. Perl, and T. H. Tan, Phys. Rev. **165**, 1466 (1968); A. B. Wicklund, G. A. Smith, W. Woischnig, S. Wojcicki, Bull. Am. Phys. Soc. **12**, 505 (1967); G. A. Smith, A. B. Wicklund, S. Wojcicki, *ibid.* **12**, 505 (1967).

[2] Previous $p+p\to$ (strange particle) experiments at moments >8 BeV/c: 10.0 BeV/c, S. O. Holmgren, S. Nilsson, T. Olhede, and N. Yamdagni, Nuovo Cimento **51**, 305 (1967); 24.5 BeV/c, J. Bartke, W. A. Cooper, B. Czapp, H. Filthuth, Y. Goldschmidt-Clermont, L. Montanet, D. R. O. Morrison, S. Nilsson, Ch. Peyrou, R. Sosnowki, A. Bigi, R. Carrara, C. Fransinetti, and I. Mannelli, *ibid.* **29**, 8 (1963); A. De Marco-Trabucco, L. Montanet, S. Nilsson, Nucl. Phys. **60**, 209 (1964).

[3] Experiments reporting possible ΛN mass enhancements at the following mass values: 2059 MeV, A. C. Melissinos, N. W. Reay, J. T. Reed, T. Yamanouchi, E. Sacharidis, S. J. Lindenbaum, S. Ozaki, and L. C. L. Yuan, Phys. Rev. Letters **14**, 604 (1965); 2098 MeV, H. O. Chon, K. H. Bhatt, and W. M. Bugg, *ibid.* **13**, 668 (1964); 2115 MeV, M. Meer, J. Mueller, M. Schneeberger, S. E. Wolf, J. Albright, E. B. Brucher, J. Lannutti, J. O'Neall, and W. H. Sims, Bull. Am. Phys. Soc. **11**, 342 (1966); 2220 MeV, T. Buran, O. Eivindson, O. Skjeffestad, H. Tofte, and I. Vegge, Phys. Letters **20**, 318 (1966); 2360 MeV, P. A. Piroue, *ibid.* **11**, 164 (1964).

[4] I. Skillicorn and M. S. Webster, BNL Bubble Chamber Report No. H10, 1962 (unpublished).

an event was found, a print was made and used to record subsequent processing of the event.

Measurement of the events was done on two conventional measuring projectors. Each track was measured in the two best stereo views for its full length or until a sagitta of more than 2 cm in space was obtained. Event measurements were required to meet certain criteria assuring adequate precision. Events failing these criteria on the previous measurement were given up to three remeasurements.

B. Event-Selection Criteria

The spatial reconstruction and kinematic fitting of the events were done by the programs EUCLID and ILLFIT, developed at the University of Illinois. Each event was examined on the scanning table by a physicist using the detailed results of the computer analysis of the event. For an event to be accepted as uniquely identified it had to meet the following criteria: (1) The χ^2 probability for the accepted mass hypothesis had to be greater than 1%. (2) The χ^2 probability of any competing hypothesis had to be at least three times less likely. (3) The ionization predictions for the accepted hypothesis had to agree with the ionization of the tracks as determined by visual inspection. If two hypotheses met criteria 1 and 3 but were within a factor of 3 in probability, they were assigned to a "twofold ambiguous" category for cross-section calculation purposes. More details of the analysis procedure are available elsewhere.[5]

III. EXPERIMENTAL RESULTS

A. Cross Sections

For purposes of calculating cross sections, the best 29 of the 41 rolls of film were chosen and a fiducial region was imposed requiring the primary vertex to lie between $X=-80.0$ cm and $X=+70.0$ cm (X is parallel to the beam with $X=0.0$ cm at the center of the chamber). Beam tracks were counted every tenth frame, yielding an extrapolation of the total track length in the fiducial region of 5.18×10^5 m. This corresponds to 1.95 events/μb.

The subsequent analysis will be restricted to events occurring in the topologies 2-prong plus V, 2-prong with kink and V, 2-prong plus 2 V's, 4-prong with kink, and 4-prong plus V.

To obtain the corrected number of events from the number of observed events, several efficiency corrections were applied. Two corrections were applied to all events: a correction for scanning efficiency of 98% and a correction for measuring efficiency of 91%. In addition, corrections for each strange-particle decay were applied to take into consideration the ratio of visible to all decays, the probability of detection of the decay inside the chamber, the loss of events due to the flight path being too short to observe, the loss of events because the kink angle was too small to observe, the chance of the final state decaying into topologies not analyzed, and the efficiency for resolving the one-constraint Σ^+ and Σ^- final states. These efficiencies are summarized elsewhere.[5] Ambiguous events were apportioned between the two final states involved in the ratio in which the final states were populated with uniquely identified events. The number of such events is given in column 3 in Table I.

Table I presents the calculated cross sections for 33 final states in which two or more events were identified in the fiducial volume. The numbers obtained for cross

TABLE I. Sample 1 lists the number of events used for cross-section calculations. Sample 2 lists the number of events used for the kinematic analysis. The errors quoted on the cross sections are statistical only.

		Sample 1			Sample 2
	Final state	Unique	Ambiguous	$\sigma(\mu b)$	Unique
1	$K^+p\Lambda$	49	7	54.4± 7.3	75
2	$K^+p\Sigma^0$	22	4	25.2± 5.0	37
3	$K^0p\Sigma^+$	8	0	14.3+ 5.1	10
4	$pp K^0\bar{K}^0$	10	0	10.4± 3.3	13
5	$K^+pK^0(n)$	12	2	25.0± 6.7	13
6	$\pi^+K^+\Lambda(n)$	100	4	101.0±10.3	100
7	$K^+p\Lambda(\pi^0)$	70	10	77.5± 8.7	95
8	$\pi^+pK^0\Lambda$	83	12	72.4± 7.4	120
9	$\pi^+pK^0\Sigma^0$	17	1	29.5± 7.0	26
10	$\pi^+\Sigma^+K^0(n)$	12	0	21.4± 6.2	18
11	$p\Sigma^+K^0(\pi^0)$	10	0	17.9± 5.7	11
12	$K^+p\Sigma^+\pi^-$	23	0	37.4± 7.8	50
13	$\pi^+K^+p\Sigma^-$	41	1	31.6± 4.9	62
14	$\pi^+pK^0\bar{K}^0(n)$	4	0	24.8±12.4	7
15	$K^+pp\pi^-\bar{K}^0$	5	0	9.8± 4.4	6
16	$\pi^+pp K^-K^0$	7	0	13.8± 5.2	12
17	$\pi^+K^+p\pi^-\Lambda$	40	6	49.0± 7.2	65
18	$\pi^+pK^0\Lambda(\pi^0)$	20	0	67.4±15.0	24
19	$\pi^+\pi^+K^0\Lambda(n)$	6	0	20.2± 8.3	9
20	$\pi^+K^+p\pi^-\Sigma^0$	16	4	21.4± 4.8	21
21	$K^+p\Sigma^+\pi^-(\pi^0)$	4	2	17.3± 7.1	7
22	$\pi^+p\Sigma^+\pi^-(K^0)$	3	1	14.7± 7.4	13
23	$\pi^+K^+\Sigma^+\pi^-(n)$	9	1	28.8± 9.1	24
24	$\pi^+K^+p\Sigma^-(\pi^0)$	19	4	22.2± 4.6	21
25	$\pi^+\pi^+p\Sigma^-(K^0)$	20	0	24.7± 5.6	28
26	$\pi^+\pi^+K^+\Sigma^-(n)$	6	1	6.8± 2.6	7
27	$\pi^+pp\pi^-K^0(K^0)$	5	0	6.3± 2.8	6
28	$\pi^+K^+p\pi^-K^0(n)$	4	0	7.8± 3.9	6
29	$\pi^+pp K^-K^0(\pi^0)$	3	0	5.9± 3.4	3
30	$\pi^+\pi^+pK^-K^0(n)$	2	0	3.9± 2.8	2
31	$\pi^+\pi^+p\pi^-K^0\Lambda$	29	1	23.1± 4.2	32
32	$\pi^+K^+p\pi^-\Lambda(\pi^0)$	34	3	39.5± 6.3	39
33	$\pi^+\pi^+K^+\pi^-\Lambda(n)$	19	0	20.3± 4.7	25
34	$K^+pp K^-$				5
35	$pp K^0K^0(\pi^0)$				1
36	$K^+pp K^-(\pi^0)$				4
37	$\pi^+K^+pK^-(n)$				11
38	$K^+pp\pi^-K^0(\pi^0)$				1

[5] M. W. Firebaugh, Ph.D. thesis, Physics Department, University of Illinois, Urbana, Illinois, 1966 (unpublished).

section purposes as described above are listed under "Sample 1." For purposes of kinematic analysis a somewhat different set of events, listed under "Sample 2," was used. Sample 2 differs from sample 1 in being drawn from the entire film and chamber volume and including only uniquely identified events (no twofold or track interchange ambiguities were included). Since the ambiguity rate was of the order of 15% or less for most final states, it is felt that no serious biases were introduced into sample 2 by this selection. The one possible exception is the $\pi^+K^+\Lambda(n)$ state in which the identity of the π^+ and K^+ was ambiguous in approximately 30% of the events. The omission of such events from sample 2 may discriminate against events with low π^+K^+ invariant mass, since in general such events had high, roughly parallel, laboratory momenta. All subsequent kinematic analysis will be based on sample 2.

An interesting feature of these cross-section data, in combination with those at lower and higher momenta, is the rapidly rising value of the $K\bar{K}$ cross section, both in absolute magnitude and relative to the total strange-particle cross section. To illustrate this, one can compute the percentage of the total identified strange-particle cross section which occurs in identified $K\bar{K}$ channels. At 5, 8, 10, and 25 BeV/c[1,2] these percentages are, respectively, 6, 12, 25, and 29%. As a particular example, the cross section for the final state $ppK^0\bar{K}^0$ has been measured at 5.0, 5.5, 8.0, and 10.0 BeV/c to be 3 ± 1, 6.4 ± 4.0, 10.4 ± 3.3, and 33 ± 16 μb, respectively, indicating a rapidly rising cross section in this momentum region.

The sum of the partial cross sections listed in Table I is about 950 μb. In addition, a record was kept of those events in which the decay vertex fit a strange-particle decay but the primary vertex permitted no good fit with zero or one unseen particle. It was assumed that such events contained more than one missing neutral particle. Using detection efficiencies similar to those for fitted events,[5] we calculated the cross section for such production to be about 590 μb. Finally, the two-prong with kink topology was scanned for and measured but not analyzed in this experiment. We estimate the cross section for this topology to be 220 μb. Similar analysis for 6-prong strange-particle events yields a cross section of 40 μb. These numbers permit an estimate of the total strange-particle production cross section of 1.8 mb, with an estimated error of 0.2 mb.

A count of all interactions over a small section of the film resulted in a measurement of the total interaction cross section for protons on protons of 39.6 ± 1.3 mb. This value agrees with previous measurements.[6]

B. General Kinematic Properties

1. c.m. Angular Distributions

Figure 1 shows the distributions of the cosine of the c.m. angle between the beam proton and various secondary particles. There were no apparent differences in the distributions between the various charge states of the pions, kaons, and nucleons, so these are plotted together. In addition, the Λ and Σ distributions were similar and are plotted together.

For low particle multiplicity the baryons are strongly collimated forward and backward while the mesons are somewhat less collimated. As the particle multiplicity increases, the peaking decreases until in the six-body final states the pions and kaons are distributed isotropically, and the baryons are distributed nearly isotropically.

This behavior may be qualitatively understood in several ways. First, as more pions are produced, i.e., the multiplicity increases, the likelihood of resonance production increases. Or conversely, the increased pion multiplicity may be due, e.g., to baryon resonance production. In either case, the decay distributions of such resonances will tend to "wash out" the forward-backward peaking of individual particles. Second, the tendency towards isotropy at high multiplicity is consistent with the idea that the more complex, highly inelastic reactions occur in the lower partial waves.

2. Transverse-Momentum Distributions

There have been several observations and speculations[7–11] on the transverse-momentum distributions for particles produced in high-energy interactions. Orear[8] points out that the two-body final-state c.m. angular distribution is well described by

$$d\sigma/d\omega \sim \exp(-P_t/0.16), \tag{1}$$

where P_t is the transverse momentum in the c.m. system in BeV/c. It has been observed[7] that over a wide range of incident energies above 25 BeV the P_t distribution for pions is given approximately by

$$N(P_t)=(P_t/P_0^2)\exp(-P_t/P_0), \quad \text{with} \quad P_0=0.18 \text{ BeV}/c \text{ at } 25 \text{ BeV}. \tag{2}$$

Although our incident energy is lower than those described in Refs. 7 and 8, we have fitted our transverse-momentum distributions with the form

$$N(P_t)=AP_t\exp(-P_t/B), \tag{3}$$

[6] W. Galbraith, E. W. Jenkins, T. F. Kycia, B. A. Leontic, R. H. Phillips, A. L. Read, and R. Rubinstein, Phys. Rev. 138, B913 (1965).

[7] C. Cocconi, L. J. Koester, D. N. Perkins, University of California Laboratory Report No. 1444, 1961 (unpublished); P. H. Fowler and D. H. Perkins, Proc. Roy. Soc. (London) 378A, 401 (1964).

[8] J. Orear, Phys. Letters 13, 190 (1964).

[9] Tai Tsun Wu and C. N. Yang, Phys. Rev. 137, B708 (1965).

[10] Kerson Huang, Phys. Rev. 156, 1555 (1967).

[11] L. G. Ratner, K. W. Edwards, C. W. Akerlof, D. G. Crabb, J. L. Day, A. D. Krisch, and M. T. Lin, Phys. Rev. Letters 18, 1218 (1967); E. W. Anderson, E. J. Bleser, G. B. Collins, T. Fujii, J. Menes, F. Turkot, R. A. Carrigan, R. M. Edelstein, N. C. Hien, T. J. McMahon, and I. Nadelhaft, *ibid.* 19, 198 (1967).

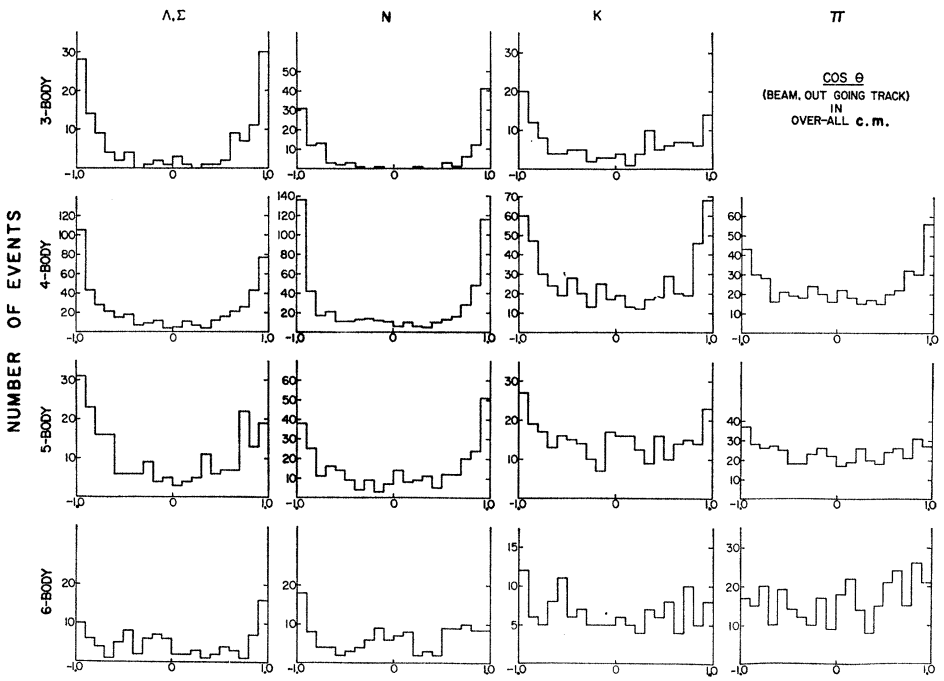

FIG. 1. Distribution in cosine of the angle in the over-all c.m. system between the incoming beam proton and outgoing particle for the various particles for varying number of bodies in the final state. All charge states of a given particle have been plotted together.

in which the best values of B were found by least squares. Figure 2 presents the data as a function of the mass of the secondary particles and the multiplicity of the final state along with the fitted curve for Eq. (3). The fitted value of the parameter B, which equals P_t at the peak of the distribution, is shown for each curve. It is seen that this expression does, in fact, represent the data fairly well for the fitted values of B indicated on the curves.

In extending such considerations to more complex

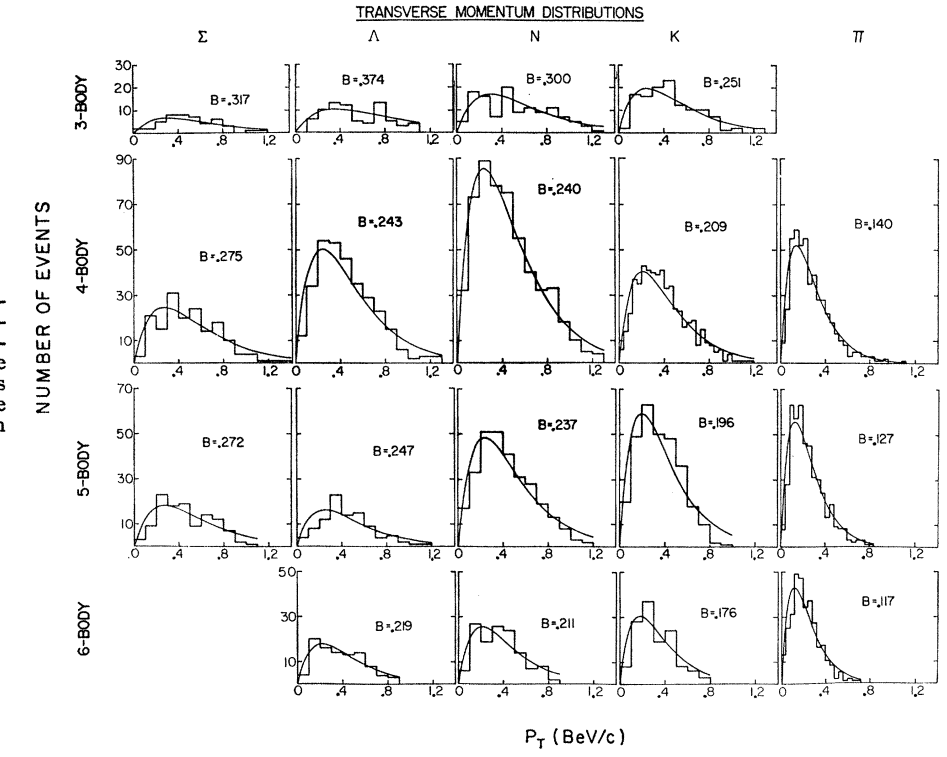

FIG. 2. Transverse momentum distributions for the various outgoing particles for varying number of bodies in the final state. The smooth curves are fits to the data of the parametric form discussed in the text.

interactions, Wu and Yang[9] suggest that for processes such as

$$A+B\rightarrow C+D+E+F, \tag{4}$$

the "falloff factor" for the sum of the magnitudes of P_t should go as

$$\exp(-\sum|P_t|/0.3), \tag{5}$$

where $\sum|P_t|$ is the sum of the magnitudes of the transverse momenta of all final-state particles. We have examined both the $\sum|P_t|$ and $\sum|P_L|$ (the longitudinal momentum in the c.m. system) distributions for our events as a function of the final-state multiplicity. The results are shown for $\sum|P_t|$ in Fig. 3. The main features of the data are the relative constancy of the central value of the distributions and the narrowing of the distributions with increasing multiplicity. The $\sum|P_L|$ distributions (not shown) shift lower with increasing multiplicity as expected.

The smooth curves on the $\sum|P_t|$ data are least-squares-fitted functions of the form

$$N(x)=A_1\rho(x)\exp(-x/A_2), \tag{6}$$

where $x=\sum|P_t|$, $\rho(x)$ is the phase-space factor for this quantity and A_1 and A_2 are free parameters. The factor $\rho(x)$ was computed by a Monte Carlo procedure with final states $KN\Lambda+n\pi$, where n runs from 0 to 3 for the three- through six-body final states (such states made up the bulk of the reactions). It is seen that the functional dependence on x suggested by Wu and Yang fits the data reasonably well if the parameter A_2 is allowed to vary. The best value of the parameter A_2 is shown for each curve.

Finally, we considered the proposal of Huang[10] that for a many-body final state the matrix element squared should be proportional to

$$\exp(-\text{const}\times\sum P_t^2), \tag{7}$$

where the sum is taken over all particles in the final state. Figure 4 presents our data for the distributions of $\sum P_t^2$. The smooth dashed curves are the least-squares-fitted functions of the form

$$N(x)=A_1\rho(x)\exp(-x/A_2), \tag{8}$$

where $x=\sum P_t^2$ over all outgoing particles, $\rho(x)$ is the phase-space factor for this quantity, and A_1 and A_2 are free parameters. The best values of A_2 are shown on the graph. It appears that this functional dependence on x does not represent the data well, particularly for the four-body final states.

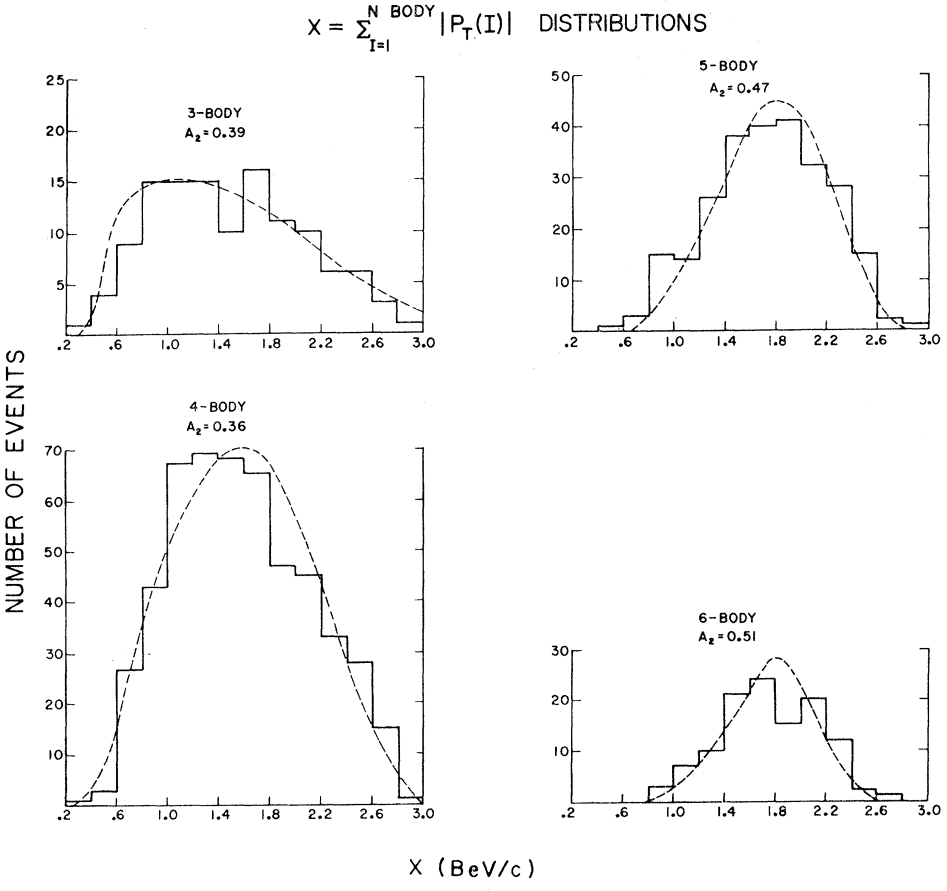

FIG. 3. Distributions for the sum of the transverse momenta over all particles in the final state. The smooth curves are fitted functions of the form $N(x)=A_1\rho(x)\exp(-x/A_2)$, where $x=\Sigma|P_t|$.

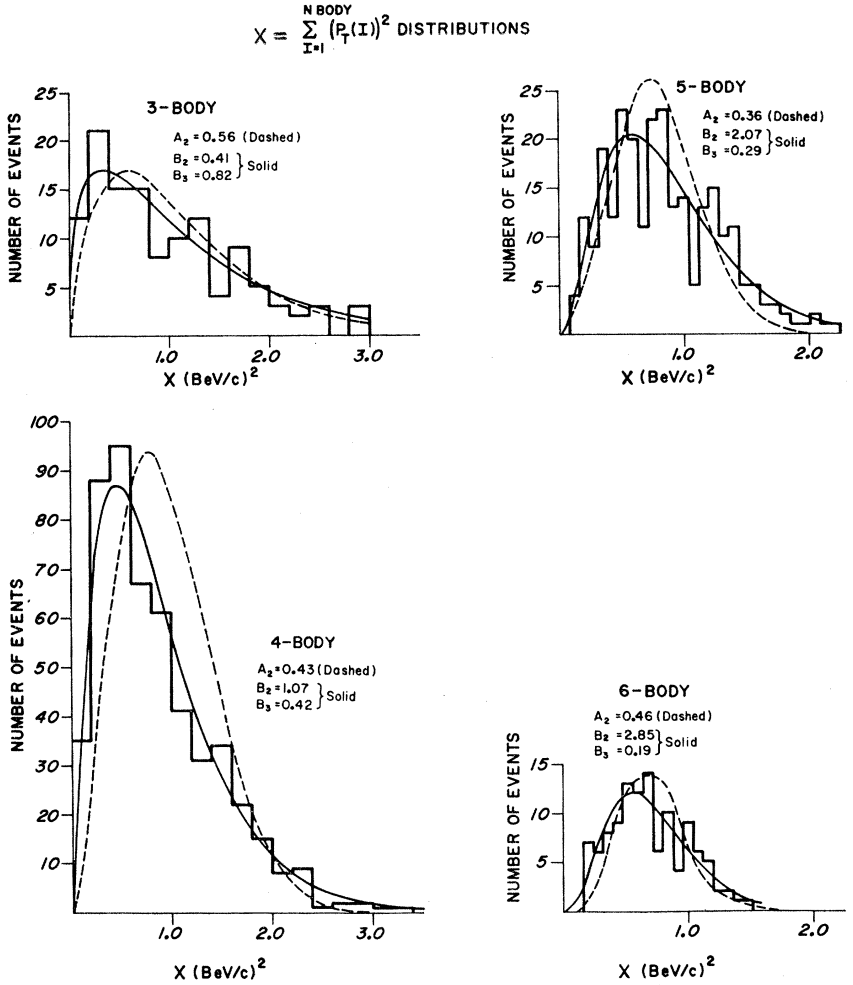

FIG. 4. Distributions for the sum of the squares of the transverse momenta over all particles in the final state. The smooth dashed curves are fitted functions of the form $N(x)=A_1\rho(x)\times\exp(-x/A_2)$, where $x=\Sigma P_i^2$ over all particles. The smooth solid curves are fitted functions of the form $N(x)=B_1x^{B_2}\exp(-x/B_3)$.

The smooth solid curves in Fig. 4 are the least-squares-fitted functions of the form

$$N(x)=B_1x^{B_2}\exp(-x/B_3), \tag{9}$$

where x is defined above and B_1, B_2, and B_3 are free parameters. This purely *ad hoc* expression represents the data quite well for the values of B_2 and B_3 shown on the curves. It has been customary to discuss distributions of transverse momenta for only those experiments in which the final states have not been uniquely identified (and hence the multiplicity is uncertain) or even, in high-multiplicity final states, in which the identity of the particles themselves may be in doubt. We present the above discussion because this experiment includes final states over a fairly wide range of known multiplicity and particle masses. It is hoped that these data may be useful for comparison with future theoretical predictions.

3. *Evidence on Dibaryon Resonances*

There have been possible $B=2, S=-1$ enhancements reported at energies of 2058, 2098, 2115, 2220, and 2360 MeV.[3] Evidence concerning the presence of such resonances in our experiment is presented in Fig. 5 in which the invariant-mass distributions for all nucleon, lambda (N,Λ), and (N,Σ) combinations are shown as a function of the final-state multiplicity. It is evident that there is no strong dibaryon resonance production present. The peaking toward the high invariant-mass end of phase space can be understood as a result of the previously discussed peripheral angular distribution of the baryons. The two baryons are usually traveling in opposite directions and so have the maximum relative energy allowed by their particular momenta.

This null result is consistent with the results reported by previous authors at lower energies.[1]

C. Detailed Final-State Analysis

1. *Three-Body Final States*

$K^+p\Lambda$. Preliminary reports on this final state have been made previously.[12] We now summarize our analy-

[12] For previous reports on the present experiment, see M. Firebaugh, G. Ascoli, E. L. Goldwasser, U. E. Kruse, L. Lavatelli, and R. D. Sard, Bull. Am. Phys. Soc. **11**, 360 (1966); M. Firebaugh, G. Ascoli, E. L. Goldwasser, and R. D. Sard, *ibid.* **12**, 45 (1967).

sis and conclusions. The dominant features of this final state are illustrated by the Dalitz plot and Chew-Low plot in Fig. 6. Clearly, the matrix element for the reaction depends on the mass of the (K^+,Λ) system, $M(K^+,\Lambda)$, and on the 4-momentum transfer to the (K^+,Λ) system, $\Delta^2(p_{\text{in}},K^+\Lambda)$, (or the equivalent 4-momentum transfer to the outgoing proton), peaking at low values of each.

In an attempt to interpret these data we have computed the predictions of the one-meson-exchange model for the two lowest mass mesons allowed, the π^0 and K^+. The Feynman diagrams for these processes are shown in Figs. 7(a) and (b). One assumes in such a model that the Δ^2 dependence at the lower vertex is that given by the Born approximation, that the propagator for a meson of mass μ is $(\Delta^2+\mu^2)^{-1}$, and that at the upper vertex the cross section for scattering of the virtual meson has the same dependence on the c.m. energy W at that vertex as does the cross section for the scattering of real mesons. Furthermore, interference terms between the diagrams shown and those with the beam and target protons interchanged are omitted since the peripheral angular distribution of the outgoing proton permits identification of the incident proton at the lower vertex.

Following the formulation of Yao,[13] we may then write the differential cross section (as a function of W

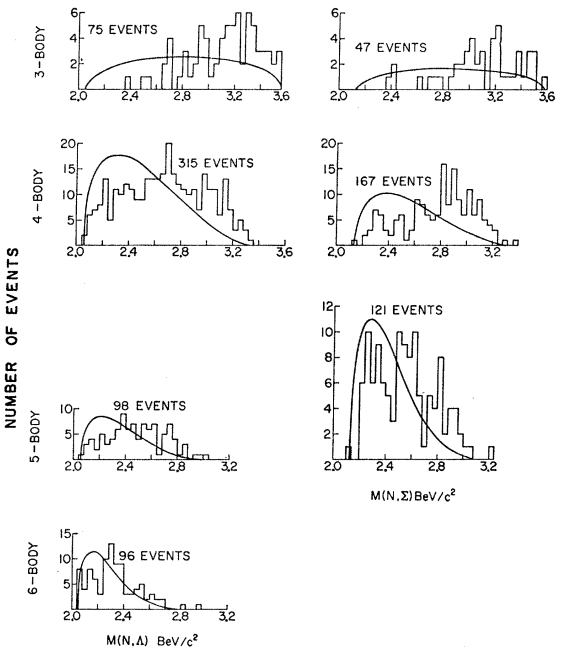

FIG. 5. Two-body invariant-mass distributions for all $B=2$, $S=-1$ combinations of the experiment. The smooth curves are the phase-space predictions, normalized to the data.

[13] Tsu Yao, Phys. Rev. **125**, 1048 (1962). The author of this paper has followed the formulation given by E. Ferrari, Nuovo Cimento **15**, 652 (1960). See also F. Salzman and G. Salzman, Phys. Rev. **120**, 599 (1960).

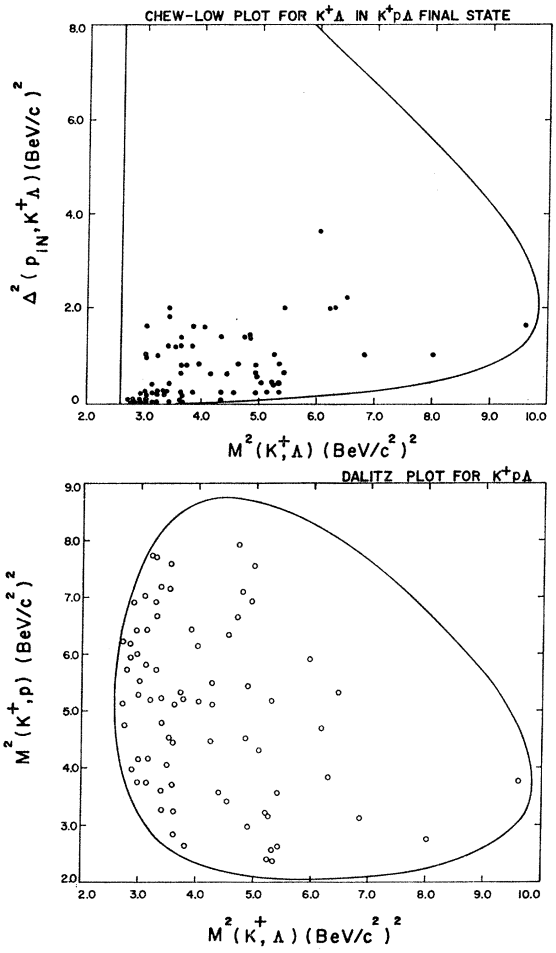

FIG. 6. Dalitz plot of $M^2(K^+,p)$ versus $M^2(K^+,\Lambda)$ and Chew-Low plot of $\Delta^2(p_{\text{in}},K^+\Lambda)$ versus $M^2(K^+,\Lambda)$.

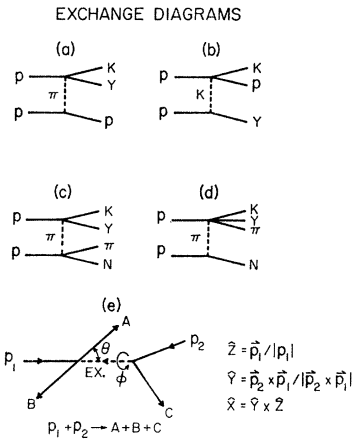

FIG. 7. Feynman diagrams for π and K exchange in the three-body final states [(a) and (b)] and for π exchange in the four-body final state [(c) and (d)]. (e) defines the coordinate system used for the decay angles (ϕ,θ) for the AB system. ϕ is measured from the X axis in the xy plane.

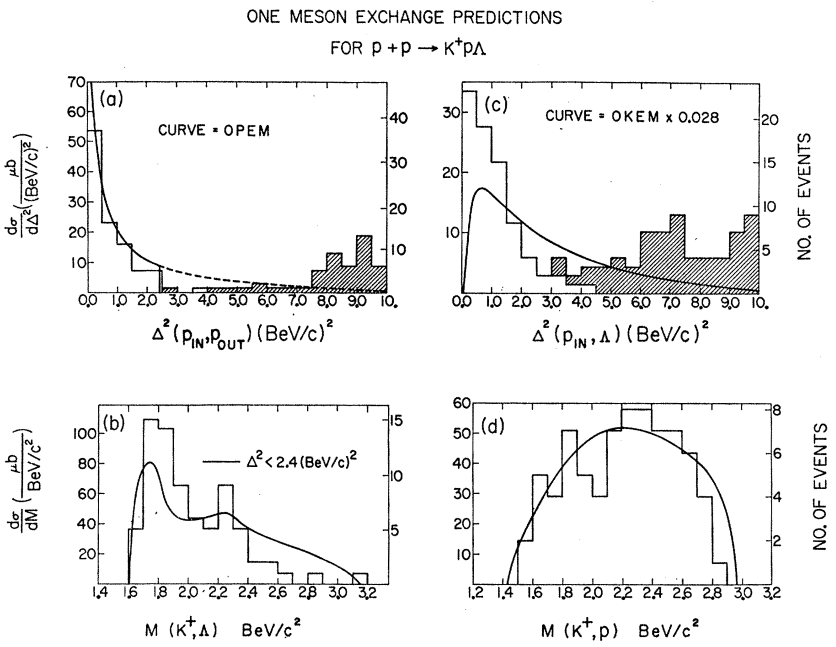

FIG. 8. Predictions of the one-meson-exchange model for the reaction $p+p \rightarrow K^+p\Lambda$. The smooth curves in (a) and (b) are the OPE predictions in absolute units and in (c) and (d) are the OKE predictions scaled down by a factor of 0.028. The open Δ^2 histograms are for the smaller of the two Δ^2 values for each event and the shaded histograms are for the larger value.

and Δ^2) as

$$\frac{d^2\sigma}{dW d\Delta^2} = \frac{1}{4\pi}\frac{G^2}{4\pi}\frac{2kW^2}{(PU)^2}\sigma_0(W)F(\Delta^2),$$

where $G^2/4\pi = 14.2$ (πNN coupling constant for OPE)[14]; $G^2/4\pi = 16.0 \pm 2.5$ [$KN\Lambda$ coupling constant for one-kaon exchange (OKE)][15]; W is the energy in the c.m. system of the upper vertex; k is the momentum of the incident particles at the upper vertex, defined by $W = (k^2+M^2)^{1/2} + (k^2+\mu^2)^{1/2}$; M is the proton mass; μ is the exchanged meson mass; P is the initial proton momentum in the c.m. system; U is the total c.m. energy,

$$\sigma_0(W) = \sigma(\pi^0 p \rightarrow K^+\Lambda) \text{ for OPE}$$
$$= \tfrac{1}{2}\sigma(\pi^- p \rightarrow K^0\Lambda) \text{ by isospin arguments;}$$
$$\sigma_0(W) = \sigma(K^+p \rightarrow K^+p) \text{ for OKE;}$$
$$F(\Delta^2) = \Delta^2/(\Delta^2+\mu^2)^2 \text{ for OPE;}$$
$$F(\Delta^2) = (\Delta^2+(M_\Lambda - M)^2)/(\Delta^2+\mu^2)^2 \text{ for OKE.}$$

This expression may be integrated numerically, using measured values for $\sigma(\pi^- p \rightarrow K^0\Lambda)$ [or $\sigma(K^+p \rightarrow K^+p)$],[16] to predict the invariant-mass and Δ^2 distributions for the K^+, Λ (or K^+p) system via the OPE (or OKE) model. In addition, the total cross section for the reaction is also predicted assuming pure exchange of each meson. Since the results of these calculations as well as later ones depend critically on the form of the input cross sections, we have shown our compilation of the data and interpolated curves in the Appendix.

The results of the calculations are shown with the data in Fig. 8. It is apparent that the shape of the $\Delta^2(p_{in},p_{out})$ prediction (OPE) agrees with the data much better than does the $\Delta^2(p_{in},\Lambda)$ curve (OKE). The $M(K^+,\Lambda)$ prediction (OPE), while not in precise agreement, does follow the general features of the data. Neither OPE curve contains any free parameters except

[14] James D. Simpson, Ph.D. thesis, Department of Physics, University of Illinois, Urbana, 1964 (unpublished).

[15] Jae Kwan Kim, Phys. Rev. Letters **19**, 1079 (1967).

[16] Sources for input cross sections for one-meson-exchange calculations: (a) $\pi^- p \rightarrow K^0\Lambda$, L. Bertanza, P. Connolly, B. Culwick, F. Eisler, T. Morris, R. Palmer, A. Prodell, and N. Samios, Phys. Rev. Letters **8**, 332 (1962); private communication from T. Binford to F. Crawford via G. Smith to M. Firebaugh; Janos Kirz, Orin I. Dahl, Lyndon M. Hardy, Richard I. Hess, and Donald H. Miller, in *Proceedings of the Thirteenth Annual International Conference on High-Energy Physics, Berkeley, 1966* (University of California Press, Berkeley, 1967); J. Steinberger, in *Proceedings of the Eighth Annual International Conference on High-Energy Physics, at CERN, 1958* (CERN Scientific Information Service, Geneva, 1958). (b) $\pi^- p \rightarrow K^0\Sigma^0$, last three references in (a); (c) $\pi^- p \rightarrow K^+\Sigma^-$, last two references in (a); R. K. Kofler, Ph.D. thesis, Department of Physics, University of Wisconsin, 1964 (unpublished); (d) $\pi^+ p \rightarrow K^+\Sigma^+$, last reference in (a); J. Bartch, L. Bonda, R. Spetch, G. Hotop, G. Knies, F. Storim, J. M. Brownlee, N. N. Biswas, D. Luers, N. Schmitz, R. Seeliger, G. P. Wolf, Nuovo Cimento **43**, A1010 (1966); David Berley and Norman Gelfand, Phys. Rev. **139**, B1097 (1965); N. L. Carayannopoulos, G. W. Tautfest, and R. B. Willmann, *ibid.* **138**, B433 (1965); S. S. Yamamoto, L. Bertanza, G. C. Moneti, D. C. Rahm, and I. O. Skillicorn, *ibid.* **134**, B383 (1964); Frank S. Crawford, Jr., Fernand Grard, and Gerald A. Smith, *ibid.* **128**, 368 (1962); Fernand Grard and Gerald A. Smith, *ibid.* **127**, 607 (1962); C. Baltay, H. Courant, W. J. Fickinger, E. C. Fowler, H. L. Kraybill, J. Sandweiss, J. R. Sanford, D. L. Stonehill, and H. D. Taft, Rev. Mod. Phys. **33**, 374 (1961); R. R. Kofler, R. W. Hartung, and D. D. Reeder, Phys. Rev. **163**, 1479 (1967); (e) $K^+p \rightarrow K^+p$, Sulamith Goldhaber, William Chinowsky, Gerson Goldhaber, Wonyong Lee, Thomas O'Halloran, Theodore F. Stubbs, G. M. Pjerrou, Donald H. Stork, and Harold K. Ticho, Phys. Rev. Letters **9**, 135 (1962); V. Cook, D. Keefe, L. T. Kerth, P. G. Murphy, W. A. Wentzel, and T. F. Zipf, Phys. Rev. **129**, 2743 (1963); J. DeBaisieux *et al.*, Nuovo Cimento **43**, 142 (1966); W. DeBaere *et al.*, *ibid.* **45**, 885 (1966); (f) $\pi^- p \rightarrow \pi^- p$ and $\pi^+ p \rightarrow \pi^+ p$, M. N. Focacci and G. Giacomelli, CERN Report No. 66-18, 1966 (unpublished).

the Δ^2 cutoff which we chose as $\Delta^2<2.4$ (BeV/c)^2, as suggested by the data. The OPE curves agree well with the data in magnitude. The OKE model, on the other hand, predicts curves about two orders of magnitude higher than the data. The measured cross section for this reaction is 54 μb: the OPE model predicts 56 μb [with $\Delta^2<2.4$ (BeV/c)^2] and the OKE model predicts 4000 μb. We conclude from the above arguments that OPE is in better agreement with these data than is OKE.

Another test of which meson is exchanged in this reaction is given by the distributions of the Treiman-Yang and "scattering" angles (ϕ,θ). These angles are defined in Fig. 7(e). If OPE applies, the angle ϕ in the $K^+\Lambda$ system should be isotropic and the $\cos\theta_\Lambda$ distribution should resemble that of real $\pi^-p\to K^0\Lambda$ scattering. If OKE applies, the angle ϕ in the K^+p system should be isotropic and the $\cos\theta_p$ distribution should resemble K^+p elastic scattering. Figure 9 shows our data. The smooth curves for the $K^+\Lambda$ system are the OPE-model predictions. The $\cos\theta_\Lambda$ distribution is the average of the measured $\pi^-p\to K^0\Lambda$ angular distributions, weighted by the $M(K^+,\Lambda)$ distribution. It is seen that the agreement with the data is only fair; the probability of the ϕ distribution being flat is 12%. The ϕ distribution suggests that other processes may be occurring, however, since the deviation from flatness seems to occur systematically at $\pm90°$. There is an indication of a similar peaking of the $M(K,\Lambda)>1.9$ BeV data at $\pm90°$ in the 5.0-BeV/c experiment,[1] whereas at 5.4 and 6.6 BeV/c[1] there may be a dip in this region of ϕ. In no case are the statistics good enough to permit definite conclusions. The smooth curves on the K^+p angular distributions are a result of the calculation described in the next section.

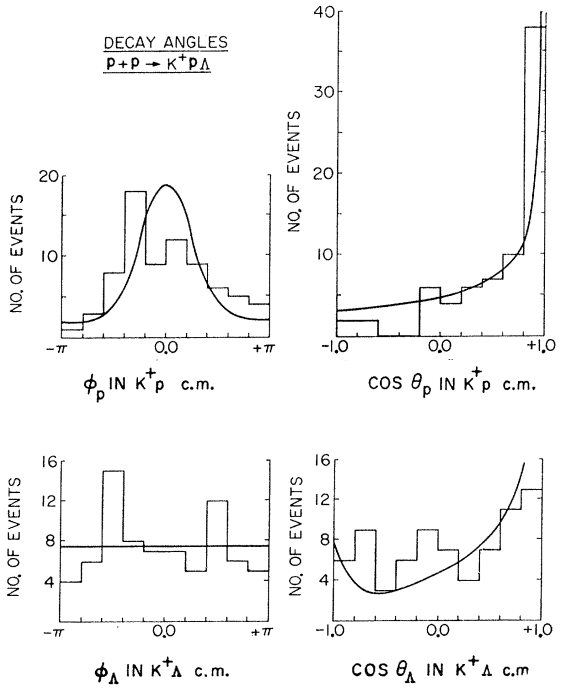

FIG. 9. Decay angular distributions for the K^+p and $K^+\Lambda$ systems in the $K^+p\Lambda$ final state. The smooth curves on the lower two histograms are the OPE model predictions normalized to the data. Those on the upper two histograms are the calculated reflections of the OPE model, normalized to the data.

The OPE model predicts directly the mass, $\Delta^2(p_{\rm in},K^+\Lambda)$, and (ϕ,θ) distributions for the $K^+\Lambda$ system. While these quantities fix the kinematics of the problem (apart from an irrelevant rotation), it is of interest to see to what extent the distributions of other kinematic quantities are the results of the observed distributions of just two of these predicted quantities, namely, $M(K^+,\Lambda)$ and $\Delta^2(p_{\rm in},K^+\Lambda)$.

We have done a Monte Carlo calculation in which events were drawn from phase space and weighted by

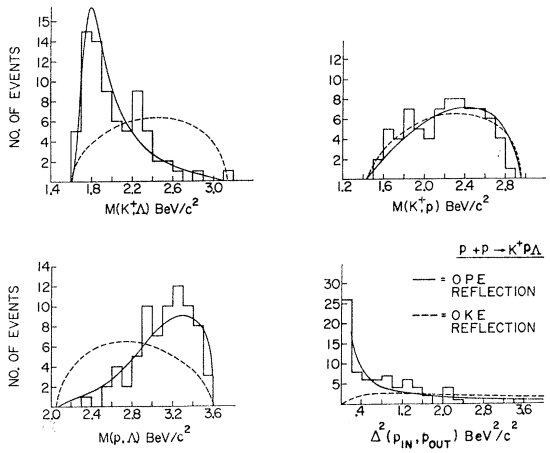

FIG. 10. Histograms of the two-body invariant-mass combinations and $\Delta^2(p_{\rm in},p_{\rm out})$ for the $K^+p\Lambda$ final state. The solid curves are the calculations for the reflections of the OPE model in which the theoretical Δ^2 distribution and parametrized $M(K^+,\Lambda)$ distribution was used. The dashed curves are the equivalent calculation for the OKE model but weighting the $M(K^+,p)$ distribution by the matrix element obtained from K^+p elastic scattering. Both sets of curves are normalized to the data.

the experimental $M(K^+,\Lambda)$ distribution in parametric form and by the theoretical Δ^2 distribution (already seen to agree well with the data). To determine the expression to use for $M(K^+,\Lambda)$, this distribution was fitted by a simple Breit-Wigner distribution times the phase-space factor, giving a good fit for the parameters $M_0=1777$ MeV and $\Gamma=345$ MeV. The calculation also assumes isotropic ϕ and $\cos\theta_\Lambda$ distributions for the $K^+\Lambda$ system. Figure 9 shows that no serious inconsistency is introduced by this assumption.

The results of this calculation are shown for the three mass distributions and for the $\Delta^2(p_{\rm in},K^+\Lambda)$ distribution in Fig. 10 and are the smooth curves on the K^+p decay angles in Fig. 9. The dashed curves in Fig. 10 are the analogous calculations for the OKE model in which the (experimental) $M(K^+,p)$ distribution has been weighted

by the measured K^+p elastic scattering cross section and the theoretical $\Delta^2(p_{\text{in}},\Lambda)$ dependence previously discussed. The good agreement of the solid curves with the data gives support to the hypothesis that the matrix element for this reaction does depend mainly on $M(K^+,\Lambda)$ and $\Delta^2(p_{\text{in}},K^+\Lambda)$. This is consistent with OPE being the dominant process in this final state.

$K^+p\Sigma^0$ and $K^0p\Sigma^+$ Final States. Since there were no apparent differences in the various distributions between the two final states, the $K^+p\Sigma^0$ and $K^0p\Sigma^+$ data have been combined for this discussion. Figure 11 shows the invariant-mass and $\Delta^2(p_{\text{in}},K\Sigma)$ distributions. In order to compare our data with the predictions of the OPE model, we have done a calculation similar to that described for the $K^+p\Lambda$ final state. Isospin considerations give the relationship

$$\sigma(\pi^0p\to K^0\Sigma^+)+\sigma(\pi^0p\to K^+\Sigma^0)$$
$$=\tfrac{1}{2}[\sigma(\pi^-p\to K^+\Sigma^-)+\sigma(\pi^-p\to K^0\Sigma^0)$$
$$+\sigma(\pi^+p\to K^+\Sigma^+)].$$

Since the cross sections on the left-hand side correspond to the $K\Sigma$ charge states summed in Fig. 11, the OPE-model predictions should be calculated using the measured cross sections on the right-hand side as input. This we have done, using the cross sections shown in the Appendix. The dashed curves for $M(K,\Sigma)$ and $\Delta^2(p_{\text{in}},K\Sigma)$ are the results of the calculation. The dashed curves for $M(K,p)$ and $M(p,\Sigma)$ are the reflections of the OPE-model predicted curves, computed by a Monte Carlo calculation (again assuming that the decay angles of the $K\Sigma$ system are isotropic). All curves shown are normalized to the data. The shape of the predictions agree fairly well with the data, with the possible exception of the 1900-MeV region in $M(K,\Sigma)$ where the peak is more pronounced than expected.

The solid curves on the mass distributions are the result of assuming that the reactions proceed 30% of the time according to phase space and 70% via the production of a $N_{3/2}^*(1924)$ resonance in the $K\Sigma$ system, of $M_0=1924$ MeV and $\Gamma=170$ MeV. They were computed by a Monte Carlo calculation using a Breit-Wigner shape with the above parameters for the $M(K,\Sigma)$ distribution and the theoretical Δ^2 dependence of the OPE model. The $\Delta^2(p_{\text{in}},K\Sigma)$ prediction of this resonance production model is quite similar to the OPE-model prediction described above. The fact that the resonance production curve agrees better with the $M(K,\Sigma)$ data in the 1924-MeV region may indicate that the input value for $\sigma(\pi^+p\to K^+\Sigma^+)$ used in our OPE-model calculation is low in this region [see Fig. 20 (a)]. In any case, the $M(K,\Sigma)$ data show a clear peak near 1924 MeV. The $\Delta^2(p_{\text{in}},K\Sigma)$ distribution indicates that the reaction proceeds via OPE. The models may well be identical in physical content since the peaking in the $\sigma(\pi^+p\to K^+\Sigma^+)$ curve at $W=1920$ can be interpreted[17] as due to the formation of the $N_{3/2}^*$-

[17] L. E. Evans and J. M. Knight, Phys. Rev. 137, B1232 (1965).

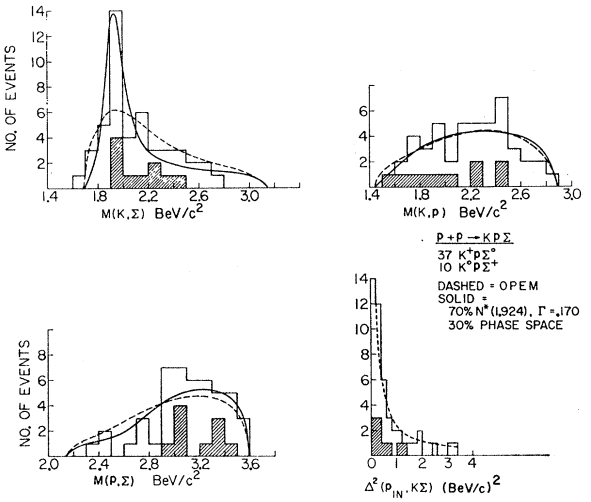

FIG. 11. Two-body invariant-mass and $\Delta^2(p_{\text{in}},p_{\text{out}})$ distributions for the $Kp\Sigma$ final states. The shaded events correspond to the $K^0p\Sigma^+$ final state. The dashed curves are the OPE model predictions and their reflections, calculated as described in the text. The solid curves correspond to the production of the $N^*(1924)$ in the $K\Sigma$ channel 70% of the time and phase space 30% of the time. All the curves are normalized to the data.

(1924). Isospin arguments show that if the reactions go by OPE through the pure $T=\frac{3}{2}$ channel, the ratio of production cross section for $pK^0\Sigma^+$ to $pK^+\Sigma^0$ should be $\frac{1}{2}$. We measure it to be 0.57 ± 0.23. While the errors are large, this result is consistent with the resonance production picture.

2. *Four-Body πKNY Final States*

$\pi KN\Lambda$ Final States. The most prominent feature of the three $\pi KN\Lambda$ final states (states 6–8 in Table I) is the strong production of the $Y^*(1385)$ and, in the $\pi^+K^0p\Lambda$ final state, the $N^*(1236)$. In addition, there is an indication of $K^*(890)$ in the $\pi^+K^0p\Lambda$ data, but little if any in the $\pi^0K^+p\Lambda$ state. The triangle plots of $M(\pi,N)$ versus $M(K,\Lambda)$ are shown in Fig. 12 for the three charge states. Any double N^* production would appear as a clustering of points in one region of these plots. There is no evidence of such quasi-two-body production.

The data also indicate the presence of a broad enhancement at low $K\Lambda$ mass as in the three-body state. We therefore parametrized this dependence by the same broad Breit-Wigner function used in the three-body final state. To determine the extent to which the above three resonances and the $K\Lambda$ enhancement contribute to each of the three charge states, we fitted simultaneously the mass distributions for each state by an incoherent superposition of four resonances plus phase space. The results of the maximum-likelihood calculation are given in Table II.

To see to what extent other kinematic quantities reflect the presence of the resonances listed in Table II, the Monte Carlo program was again used to generate the curves in Figs. 13 and 14. One obvious effect is the

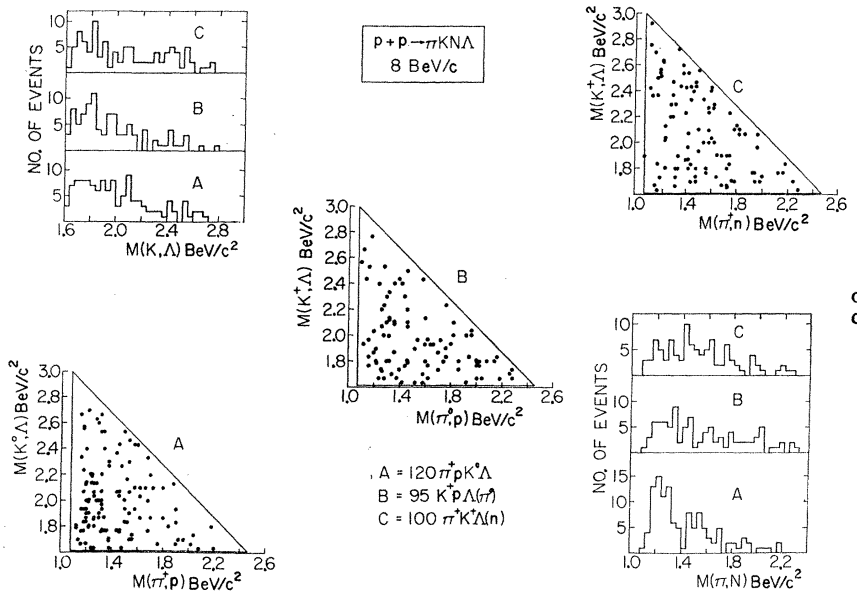

FIG. 12. Scatter plots and histograms of $M(\pi,N)$ and $M(K,\Lambda)$ for the three charge states of $\pi KN\Lambda$.

peaking of the Trieman-Yang angle at $\phi_N=0°$ in the πN system due to the $\pi\Lambda$ resonance at 1385 MeV and an equivalent peaking at $\phi_\Lambda=0°$ in the $\pi\Lambda$ system of the $\pi^+K^0p\Lambda$ final state due to the π^+p resonance at 1236 MeV. Figure 13 shows the (ϕ,θ) angular distributions for the $\pi\Lambda$ and πN systems. Good agreement between the data and calculation is evident. The shaded histograms in the πN distributions are for those events not containing a $Y^*(1385)$ [$M(\pi,\Lambda)>1485$ MeV or <1285 MeV] and in the $\pi\Lambda$ distributions are for those events not containing a $N^*(1236)$ in the π^+p channel [$M(\pi^+,p)>1.356$ MeV or <1116 MeV]. These data confirm the above conclusion. The flat Treiman-Yang distribution for the πN systems in which the $Y^*(1385)$ has been omitted is consistent with OPE being the mechanism giving rise to these events.

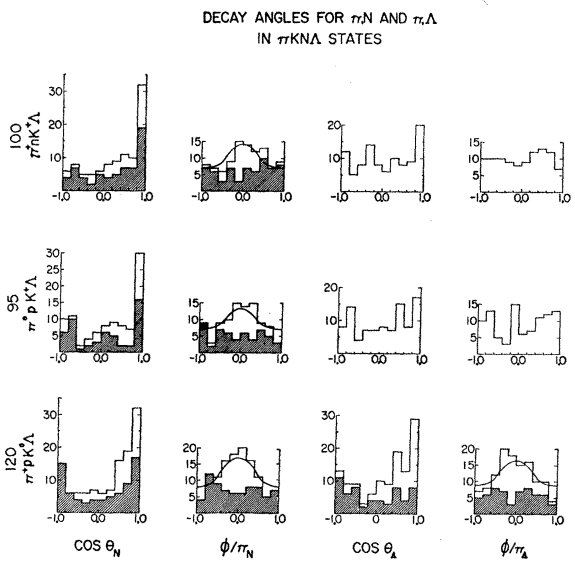

FIG. 13. Decay angles for the πN and $\pi\Lambda$ combinations in the three charge states of the $\pi KN\Lambda$ final state. The shaded πN events are those in which the $Y^*(1385)$ has been excluded by a mass cut of $M(\pi,\Lambda)>1485$ or <1285 MeV. The shaded $\pi\Lambda$ events are those in which the $N^*(1236)\pi^+p$ region has been excluded by the mass cut $M(\pi^+,p)>1356$ MeV or <1116 MeV. The smooth curves are resonance reflection calculations which account for the peaking in the Treiman-Yang angle at 0°.

Experimentally it was noted that the c.m. opening angle between the Λ particle and nucleon was much more peaked near 180° for the final states $\pi^+K^0p\Lambda$ and $\pi^0K^+p\Lambda$ than it was for the $\pi^+K^+n\Lambda$ state. This caused the Λp mass distributions to peak at higher mass values than the Λn distribution. To simulate this peaking in the $p\Lambda$ opening angle in the Monte Carlo calculation, we parametrized the experimental dependence to the Λ and outgoing proton and folded them into the calculation for the $\pi^+K^0p\Lambda$ and $\pi^0K^+p\Lambda$ states.[18] In Fig. 14 all two-body mass distributions are displayed along with the results of the calculations.

TABLE II. Results of maximum-likelihood fits for $\pi KN\Lambda$ states

	$\pi^+K^0p\Lambda$ (%)	$\pi^0K^+p\Lambda$ (%)	$\pi^+K^+n\Lambda$ (%)
$K^*(890)$	15.5±6.1	1.9± 6.8	···
$N^*(1236)$	34.2±7.4	10.2± 7.9	5.0± 5.9
$Y^*(1385)$	29.1±6.8	37.7±12.0	33.8± 7.4
$M(K,\Lambda)$	15.6±9.1	50.7±19.2	18.1±11.1
$M_0=1777$ MeV			
$\Gamma^0=345$ MeV			
Phase space	5.7	0.0	43.1

[18] The parametric form used for the dependence on the Δ^2 to the proton was $\exp(-0.87\Delta^2)$ and for the Λ, $\exp(-1.2\Delta^2)$. These were obtained by a rough fit to the data.

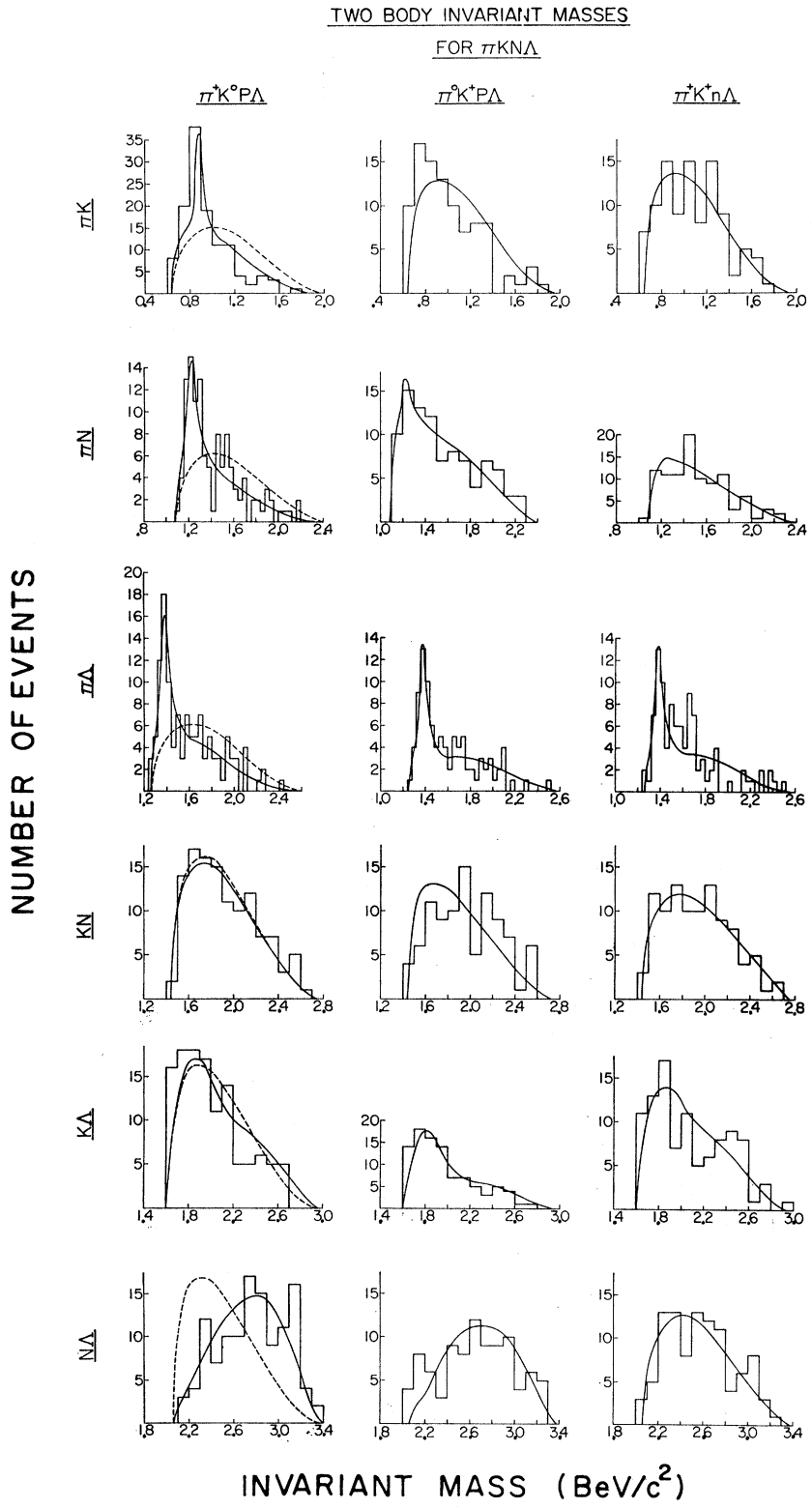

FIG. 14. Two-body invariant masses for the three charge states of $\pi KN\Lambda$. The dashed curves on the $\pi^+K^0p\Lambda$ data are the phase-space predictions. The smooth curves are the result of calculations assuming the amounts of the four resonance shapes listed in Table II. In addition, the $\pi^+K^0p\Lambda$ and $\pi^0K^+p\Lambda$ final states have the experimental Δ^2 dependence to the outgoing baryons included to give the correct $M(p,\Lambda)$ dependence.

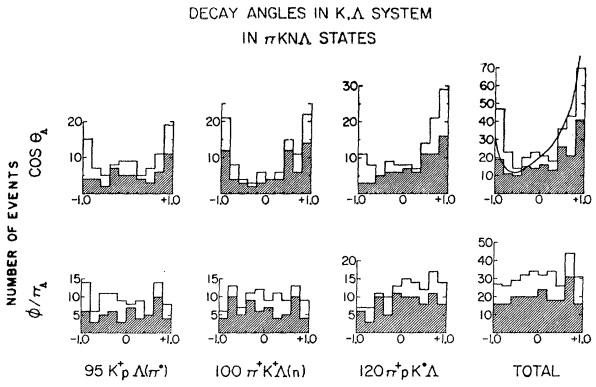

FIG. 15. Decay angles for the $K\Lambda$ system in $\pi KN\Lambda$ final states. The shaded events are those excluding the $Y^*(1385)$ by a mass cut $M(\pi,\Lambda)>1485$ MeV or <1285 MeV. The smooth curve on the total $\cos\theta_\Lambda$ distribution is obtained by weighting the real $\pi^-p\to K^0\Lambda$ angular distributions by the $M(K,\Lambda)$ distribution.

In Fig. 15 we show the (θ,ϕ) angular distributions for the K,Λ systems. For those events proceeding via the OPE process shown in Fig. 7(c), the ϕ distribution should be flat and the $\cos\theta$ distribution should resemble real $\pi^-p\to K^0\Lambda$ inelastic scattering (shown as the smooth curve on the total $\cos\theta$ data). The ϕ distributions is consistent with isotropy and the agreement between the real scattering and our data appears good. This is somewhat unexpected due to that fact that the total sample plotted contains many $Y^*(1385)\pi\Lambda$ combinations which could be produced via OPE only through the diagram shown in Fig. 7(d). The shaded events in Fig. 15 are those not containing the $Y^*(1385)$. This cut, by eliminating events arising from Fig. 7(d), should enhance the agreement between the data and the real $\pi^-p\to K^0\Lambda$ scattering angular distribution. It appears however, that the agreement between the $\cos\theta_\Lambda$ distribution of events remaining after this cut and the real pion scattering distribution is somewhat poorer than that between the whole sample and real pion scattering.

We conclude the discussion of the $\pi KN\Lambda$ final states by examining the data to see whether they suggest the presence of $Y^*(1680)$ in the $\pi\Lambda$ channel. This recently discovered resonance[19,20] has a mass of 1683 ± 15 MeV and a width of 120 ± 30 MeV. Figure 16 shows the total $M(\pi,\Lambda)$ distribution for the three charge states. The smooth curve is the result of a two-parameter fit in which the amounts of the $Y^*(1385)$ and $Y^*(1680)$ are allowed to vary while the masses and widths are held constant at $M_1=1385$, $\Gamma_1=80$, $M_2=1680$, and $\Gamma_2=140$ MeV. The best values for the percentages of $Y^*(1385)$ and $Y^*(1680)$ are $(36.1\pm5.5)\%$ and $(10.9\pm4.7)\%$, respectively.[21]

It is possible that we are observing a threshold effect in the pp experiment similar to that observed in K^-p experiments. In K^-p data, no $Y^*(1680)$ is present at 4.1 BeV/c momentum, but at 5.5 and 6.0 BeV/c [19,20] it is produced. In p-p data, none is produced at 5.0 or 5.5 BeV/c and little if any at 6.6 BeV/c,[1] while at 7.87 and 10.0 BeV/c this resonance may be present. In view of the paucity of the data and uncertainty in the background, this is hardly a conclusive result.

$\pi KN\Sigma$ Final States. This configuration of particles was analyzed in the five charge states 9–13 in Table I. One would expect *a priori* the production of the allowed N^*, K^*, and Y^* resonances in a manner similar to the production observed in the $\pi KN\Lambda$ charged states. It appears, however, that an even simpler picture of virtual pion scattering via Fig. 7(c) explains the data satisfactorily.

In Fig. 17 we show the $M(\pi,N)$ and $M(K,\Sigma)$ distributions for these events. It is apparent that there is strong $N^*(1236)$ production in the $T=\frac{3}{2}$ state. In addition, the $K\Sigma$ systems peak strongly in the low-mass region.

Since there is little, if any, $K^*(890)$, $Y^*(1405)$, or $Y^*(1660)$ produced, we assumed that there was little contribution to these reactions from Fig. 7(d). To see what the simple OPE model via Fig. 7(c) predicted for the $M(\pi,N)$ and $M(K,\Sigma)$ distributions, we performed the following calculation. Using our compilation of the data on the cross sections for $\pi^+p\to\pi^+p$, $\pi^-p\to\pi^-p$,

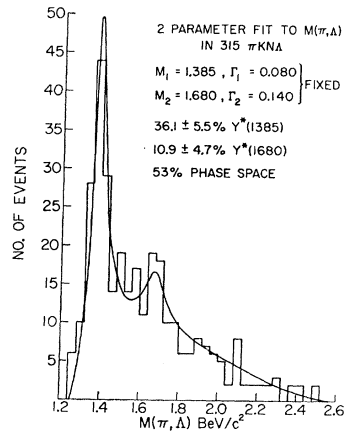

FIG. 16. Histogram of $M(\pi,\Lambda)$ for all $\pi KN\Lambda$ events. The smooth curve is the result of a two-parameter fit to the data in which the amounts of $Y^*(1385)$ and $Y^*(1680)$ are the free parameters. The resulting parameters are shown.

[19] M. Derrick, T. Fields, J. Loken, R. Ammar, R. E. P. Davis, W. Kropac, J. Mott, and F. Schweingruber, Phys. Rev. Letters **18**, 266 (1967).

[20] D. C. Colley, F. Macdonald, B. Musgrave, W. M. R. Blair, I. S. Hughes, R. M. Turnbull, S. J. Goldsack, K. Paler, L. K. Sisterson, W. Blum, W. M. N. Allison, D. H. Locke, L. Lyons, P. J. Finney, C. M. Fisher, and A. M. Segar, Phys. Letters **24B**, 489 (1967).

[21] The expression used to fit the data was

$$Y(M)=a_1\times(\text{phase space})+a_2\times[\text{Breit-Wigner (1385, 80)}]\times(\text{phase space})+a_3\times[\text{Breit-Wigner (1680, 140)}]\times(\text{phase space}),$$

with $a_1=1.0-a_2-a_3$.

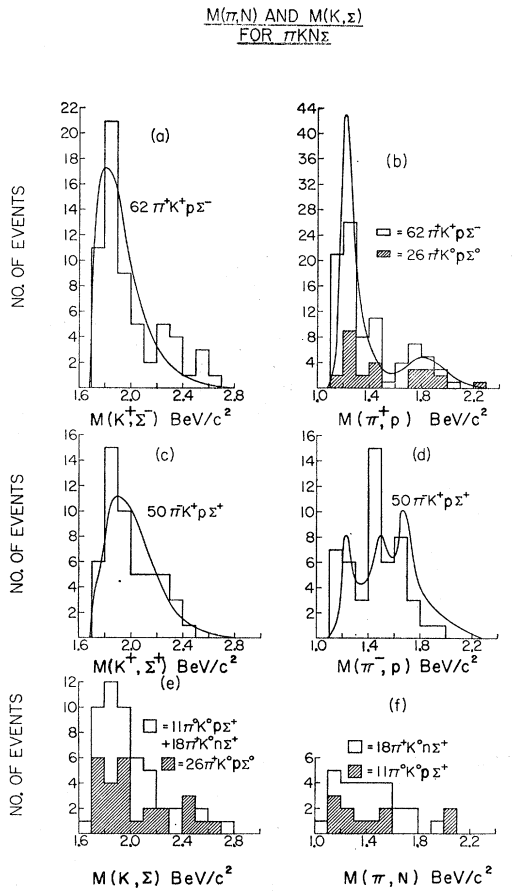

FIG. 17. Distributions of $M(\pi,N)$ and $M(K,\Sigma)$ for five $\pi KN\Sigma$ final states. The smooth curves are the OPE model calculations in which real scattering cross sections are used at each vertex. The smooth curves are normalized to the data.

$\pi^+p \to K^+\Sigma^+$, and $\pi^-p \to K^+\Sigma^-$ (see the Appendix), we computed the matrix element squared for these scattering processes.[22] It was then assumed that the matrix element for $p+p \to \pi KN\Sigma$ was just the product of the appropriate matrix elements at both vertices (from real pion scattering) and the pion propagator. A Monte Carlo calculation was done in which events drawn from phase space were weighted by the square of this matrix element. The smooth curves in Fig. 17 are the results of the calculation for the reactions $p+p \to \pi^+K^+p\Sigma^-$ and $p+p \to \pi^-K^+p\Sigma^+$. Since the $\sigma(\pi^-p \to K^+\Sigma^-)$ and $\sigma(\pi^-p \to K^0\Sigma^0)$ curves do not differ greatly, the π^+p combinations for the $\pi^+pK^0\Sigma^0$ events are shown (shaded) in the π^+p graph [Fig. 17(b)]. No attempt has been made to preserve the absolute normalization of the curves (the curves shown are normalized to the data), but it appears that the shape of the curves agrees quite well with the data.

This model predicts certain decay angular distributions. Namely, the ϕ distribution for the πN and $K\Sigma$ systems should be flat and the $\cos\theta$ distributions should resemble real πp scattering. In Fig. 18 we show the decay distributions for these systems. The smooth $\cos\theta_P$ curve on the π^+p data is the result of weighting the observed π^+p elastic scattering angular distributions by our observed $M(\pi^+,p)$ distribution. The smooth curve on the mixed isospin πN combinations is the observed π^-p elastic scattering data weighted by the πN spectrum. Since the $\cos\theta_N$ distributions for the three charge states involved were not noticeably different, they have been added. The smooth curves on the $K^0\Sigma^0$ and $K^0\Sigma^+$ $\cos\theta$ distributions are generated in the same manner, with the smooth curve being the weighted measured $\pi^-p \to K^0\Sigma^0$ angular distribution. We observe that these angular distributions also seem to agree with the simple OPE-model picture.

One distribution not fully accounted for by this model is the $N\Sigma$ mass distribution (see Fig. 5 for the total) which is more peaked toward the high-mass end of phase space than predicted. The model has not fully taken into account the peripheral nature of the baryon angular distributions which gives rise to this effect. However, the conclusion that we draw from the generally good agreement between the data and this

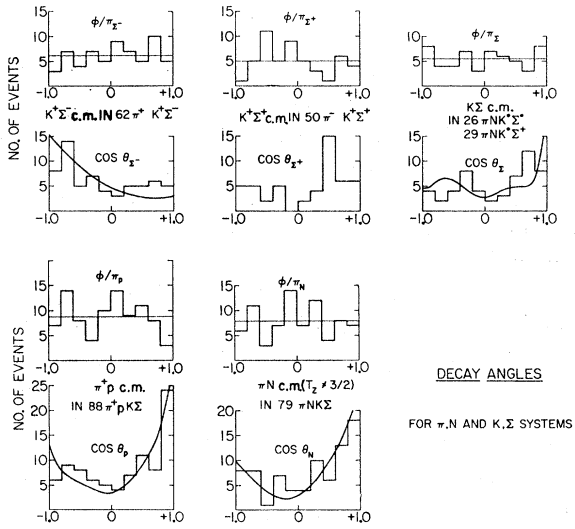

FIG. 18. Decay angular distributions for πN and $K\Sigma$ systems in the $\pi KN\Sigma$ final states. The smooth curves on the $\cos\theta$ histograms for the $K^+\Sigma^-$ and π^+p systems are the result of weighting the observed real scattering angular distributions by their respective mass distributions. The smooth curve for the 26 $K^0\Sigma^0$ and 29 $K^0\Sigma^+$ events corresponds to weighting the observed $\pi^-p \to K^0\Sigma^0$ angular distribution by the combined mass distribution. The smooth curve on the 79 πN events results from weighting the measured π^-p elastic scattering angular distribution by the total mass distribution.

[22] The matrix element was derived from the cross section by $M(W)^2=(p/q)W^2\sigma(W)$, where p is the initial c.m. momentum, q is the final c.m. momentum, and W is the energy in the c.m. system.

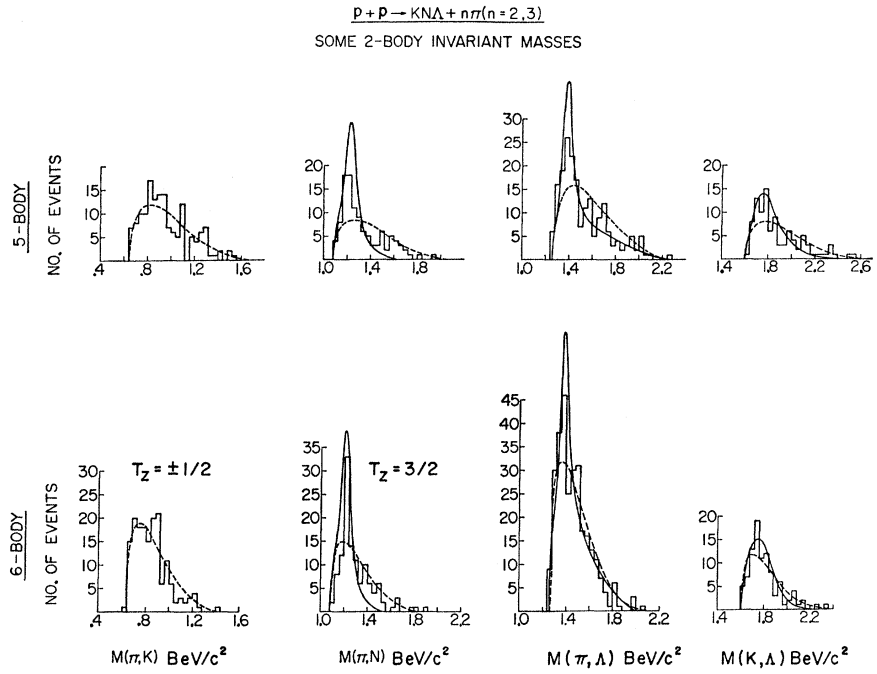

FIG. 19. Some two-body invariant-mass distributions in the five- and six-body final states. The dashed curves are the phase-space predictions. The smooth curves result from assuming that the reaction proceeds completely through resonance production in the mass combination displayed.

simple theory is that OPE explains the main features of our $\pi KN\Sigma$ final-state data and that the virtual pion involved in the scattering behaves very much like a physical pion.

3. *Five- and Six-Body Final States*

The following discussion will be based on the 119 events in the final states 17–20 and on the 96 events in final states 31–33 (Table I). Since the complexity of the analysis increases rapidly with increasing particle multiplicity, no detailed analysis has been attempted. We can, however, draw certain conclusions on the production mechanism for these final states.

In Fig. 19 we show some of the more interesting two-body invariant-mass combinations for these final states. Since the distributions are similar for the various isospin states, they have been added together. The dashed curves are the phase-space predictions and are normalized to the data. The solid curves, when shown, are the results of a calculation assuming production of the invariant mass shown proceeds via 100% resonance formation, i.e., that every event included one resonant pair of particles. The parameters for the simple Breit-Wigner forms used were: for $T=\frac{3}{2}\pi N$, $M_0=1213$ MeV, $\Gamma=120$ MeV; for $\pi\Lambda$, $M_0=1385$ MeV, $\Gamma=80$ MeV; and for the $K\Lambda$ combinations, $M_0=1777$ MeV, $\Gamma=345$ MeV.

These data show that K^* production is weak while $N^*(1236)$ and $Y^*(1385)$ resonances are strongly produced. In fact, the data indicate that essentially all of the five- and six-body production observed involves formation of these two baryon resonances, with some contribution due to the $K\Lambda$ enhancement. We have also seen an indication that the recently observed[23] $N^*(2050)$ is present in the $\pi K\Lambda$ mass distributions in about 30% of both five- and six-body states. The data relevant to this effect will be presented in a separate publication.

IV. CONCLUSIONS

The total strange-particle production cross section is estimated at 1.8 ± 0.2 mb with about half the production occurring in final states identified in this experiment. $K\bar{K}$ production is higher than at lower momenta but is still too small to provide adequate statistics for a detailed analysis. The NY mass spectra were examined for possible dibaryon resonances and none was found. The NY mass spectra peak at the high end because of the peripheral nature of the baryon angular distributions. OPE explains the $K^+p\Lambda$ and, qualitatively, the $\pi KN\Sigma$ final states but may not account for all of the $K\Sigma$ peak at 1924 MeV in the $Kp\Sigma$ final states. The $\pi KN\Lambda$ and the five- and six-body final states examined are more complex and involve production of the

[23] R. R. Kinsey, W. Chinowsky, P. Condon, S. Klein, M. Mandelkern, P. Schmidt, J. Schultz, F. Martin, M. L. Perl, and T. H. Tau, Bull. Am. Phys. Soc. 12, 916 (1967).

$N^*(1236)$ and $Y^*(1385)$. Finally, in all states including a K and Λ we observe a broad enhancement at low $K\Lambda$ masses which may be characterized by a Breit-Wigner shape, with $M_0=1777$ MeV and $\Gamma=345$ MeV. OPE, with the K and Λ originating at the same vertex, is probably a dominant mechanism in the production of these final states.

ACKNOWLEDGMENTS

We wish to thank D. Rahm and M. Webster for their help in tuning the beam, and the operating staff of the beam and of the 80-in. bubble chamber, and the AGS without whose fine cooperation this experiment would not have been possible. We are indebted to our scanning and measuring personnel and the IBM 7094 staff for their efforts throughout the experiment. We thank L. Lavatelli and R. Hanft for their help in various stages of the experiment and, finally, R. K. Logan, T. A. O'Halloran, and J. D. Jackson for useful discussions on the interpretation of the data.

APPENDIX

Since the one-meson-exchange calculations discussed in the text depend rather critically upon the input cross sections used, we present in Fig. 20 the compilation of data and the (freehand) curves that we used to represent them. No claim is made for their accuracy or completeness, and they are presented simply to indicate the input for our calculations. They are drawn from sources listed in Ref. 16.

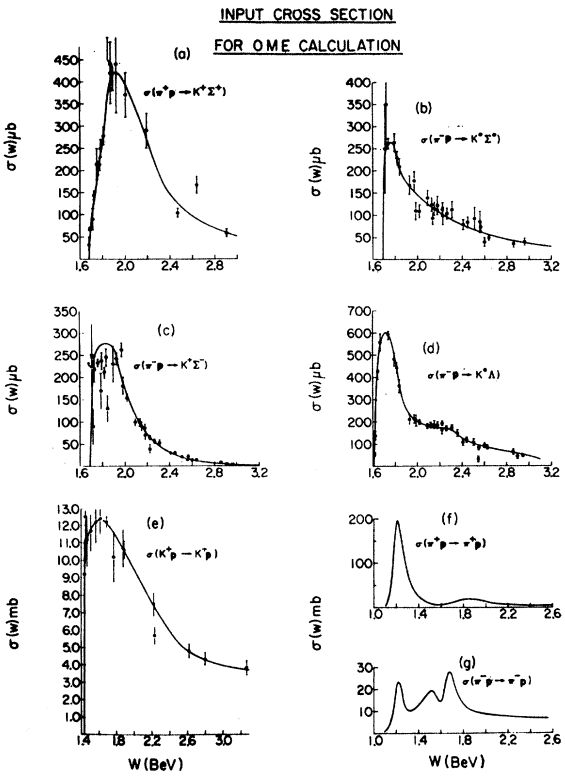

FIG. 20. Compilation of data and freehand interpolation for various cross sections for scattering processes used in one-meson-exchange calculations in the test. Sources of the data are given in Ref. 16.